Influence of alluvial slope on avulsion in river deltas

Octria A. Prasojo[1,2], Trevor B. Hoey[3], Amanda Owen[1] and Richard D. Williams[1]

[1]School of Geographical and Earth Sciences, University of Glasgow, University Avenue, Glasgow, G12 8QQ, United Kingdom
[2]Geoscience Study Program, Faculty of Mathematics and Natural Sciences (FMIPA), Universitas Indonesia, Depok 16424, Indonesia
[3]Department of Civil and Environmental Engineering, Brunel University London, Uxbridge, UB8 3PH, United Kingdom

Correspondence to: Octria A. Prasojo (octria.prasojo@glasgow.ac.uk)

Abstract. Changing hydrological regimes, sea-level rise, and accelerated subsidence are all putting river deltas at risk across the globe. One mechanism by which deltas may respond to these stressors is that of avulsion. Decades of delta avulsion studies have resulted in conflicting hypotheses as to whether avulsion timing and location are primarily controlled by upstream (water and sediment discharge) or downstream (backwater and sea-level rise) drivers. Here we use Delft3D morphodynamic simulations to test the upstream-influence hypothesis by varying the initial alluvial slopes upstream of a self-formed delta plain within a range (1.13×10^{-4} to 3.04×10^{-3}) that is representative of global deltas, while leaving all other parameters constant. Avulsion timing and location were recorded in six scenarios modelled over a 400-year period. We measured independent morphometric variables including avulsion length, delta lobe width, bankfull depth, channel width at avulsion, delta topset slope and sediment load and compare these to natural and laboratory deltas. We find that larger deltas take more time to avulse as avulsion timing scales with avulsion length, delta lobe width and bankfull depth. More importantly, we find strong negative correlations between sediment load-avulsion timescale and sediment load-initial alluvial slope. Sediment load is directly dependent on the upstream alluvial slope, and increases in this slope raise transport capacity and introduce more sediment into a delta plain leading to higher aggradation rates and, consequently, more frequent avulsions. These results induce further debate over the role of downstream controls on delta avulsion.

1 Introduction

River deltas are home to ~339 million people worldwide, are hotspots for biodiversity, and are crucial carbon sinks (Ericson et al., 2006; Hackney et al., 2020; Loucks, 2019; Shields et al., 2017; Syvitski and Saito, 2007). However, the geomorphic dynamism of river deltas has been, and continues to be, altered by amplifying stressors such as changing hydrological regimes, sea-level rise, and accelerated subsidence, putting human and other systems that rely on river deltas at considerable risk (Giosan et al., 2014; Syvitski et al., 2009; Tessler et al., 2015; Wallace et al., 2014). A frequently observed and geologically rapid mechanism by which deltas respond to these stressors is by river flow avulsing from one distributary channel into another. Delta avulsion location correlates with backwater length, slope break and valley exit location measured from the shoreline (Ganti et al., 2016a; Hartley et al., 2017; Prasojo et al., 2022). Many studies have proposed different hypotheses for the main

controls of delta avulsion frequency (e.g. Aslan et al., 2005; Brooke et al., 2020; Edmonds et al., 2009; Kleinhans & Hardy, 2013; Nijhuis et al., 2015; Slingerland & Smith, 2004), but there is currently no consensus over the conditions under which the various driving factors control this frequency.

35 During avulsion, flow is abruptly diverted out of an established river channel into a new course on the adjacent floodplain or delta plain (Jones and Schumm, 2009; Slingerland and Smith, 2004). When a delta channel avulses, the population, infrastructure and economic activities on the delta plain may be at risk. Delta lobe-scale avulsions may be considered rare, but this is partly due to anthropogenic controls on many delta channels preventing avulsion (e.g. built riverbanks), and unmodified systems can exhibit avulsion over decadal or shorter timescales, for example once every 12 years in the Yellow River Delta (Jerolmack, 2009) or 4 years in Sulengguole River, China (Li et al., 2022). Avulsions may be full, where the flow following a

40 new course completely abandons its parent channel, or partial in which only a portion of the flow is diverted (Slingerland and Smith, 2004). Avulsion is often effectively instantaneous but may also be gradual as in the Rhine-Meuse delta, where one documented avulsion event took 1250 years to complete (Stouthamer & Berendsen, 2001). There are also several styles of avulsion: annexation, in which a pre-existing channel is reoccupied; incision, where a new channel is scoured into the floodplain surface as a direct result of the avulsion; and progradation, where extensive sediment deposition, such as a mouth

45 bar, causes flow bifurcation and formation of a multi-channelled distributive network (Slingerland and Smith, 2004).

River deltas are initiated through repeated mouth bar deposition due to sudden expansion and deceleration of a sediment-laden jet of water entering relatively still water, usually a sea or lake (Bates, 1953; Edmonds et al., 2011; Kleinhans et al., 2013; Wright, 1977). Mouth bars grow in both upstream and downstream directions from the point of initiation. Once a mouth bar's aggradation reaches 40-60% of the initial flow depth, it will stop growing because the sediment is advected around the bar

50 rather than accelerated over it (Edmonds and Slingerland, 2007; Fagherazzi et al., 2015; Kleinhans et al., 2013). This cessation of bar growth is the point where avulsion by progradation or bifurcation starts in a river delta. Simultaneously, avulsion by incision takes place in the proximal parts of a delta plain when mouth-bar deposition and stagnation induce parent channel backfilling or in-channel aggradation, triggering an avulsion to create a smaller distributive channel network by breaching the channel levee (Ganti et al., 2016a). The location of the point furthest upstream where a delta channel starts to avulse correlates

55 with the location of a break (i.e. decrease) in bed slope (Prasojo et al., 2022; Ratliff et al., 2021), the limit of the backwater zone (Brooke et al., 2022; Ganti et al., 2016a), and the exit point from the river valley (Hartley et al., 2017).

A study of 105 global river deltas found that the strongest correlation is between the locations of avulsion nodes and of the decreases in slope at the transition from an alluvial to a delta slope (Prasojo et al., 2022). Consequently, it is hypothesised that the slope of the alluvial river upstream of a delta controls the frequency of avulsion on delta plains, with steeper alluvial slopes

60 leading to more frequent avulsions. This control is due to greater sediment transport capacity on steeper slopes (Bagnold, 1966) such that, subject to sediment availability, more sediment per unit width will be delivered to a delta plain where alluvial slopes are steeper. Assuming constant channel width and no subsidence, any reduction in stream power across the delta plain leads to aggradation, the rate of which will be greater when upstream sediment supply is higher, which in turn leads to increased

avulsion frequency (Jerolmack & Mohrig, 2007; Mohrig et al., 2000). Alternatively, lower alluvial slopes are associated with lower sediment input flux and hence less frequent avulsion.

To test if the alluvial slope upstream of a delta controls the timing of avulsion on delta plains, we use Delft3D morphodynamic simulation software to: 1) assess the effect of varying alluvial slopes upstream of a delta slope break on the avulsion timescale; and, 2) investigate the primary controls over delta avulsion. Morphometric variables (delta lobe width, channel width at avulsion, avulsion length, topset slope, bankfull depth and sediment supply) were measured at every timestep during delta growth. These morphometric properties are measured as independent variables expected to covary with avulsion timescales. This investigation aims to: (1) identify the role of alluvial slope upstream of delta plains on avulsion timescales; (2) explain the mechanisms by which the controlling variables determine avulsion timescale; and, (3) compare avulsion timescales from this numerical model with an analytical solution and also with observations from natural and physical experimental river deltas. A robust understanding of these processes has practical implications due to their direct impact on coastal and inland flood risk on highly populated river deltas, as well as contributing to a fundamental understanding of natural delta building processes.

2 Methods

We designed a set of numerical experiments to model a natural scale river delta (7.5 x 7.5 km, 300 by 300 computational cells, each $625m^2$) using Delft3D (v.4.04.02) software. For comparability with previous studies, we adopted physical parameters used in similar Delft3D river delta models by Edmonds & Slingerland (2010) and Caldwell & Edmonds (2014). Model bathymetry was designed to accommodate the six alluvial slopes defined below as our model scenarios.

2.1 Scenario definition

The model used a range of alluvial slopes upstream of the delta's slope break ($S_{alluvial}$) (Fig. 1a), which are considered to be representative of natural river deltas (Fig. 1b). Representative percentiles of the ratio between $S_{alluvial}$ and downstream delta topset slope (S_{topset}) were determined from 105 global river deltas measured by Prasojo et al. (2022) (Fig. 1b; Table 1). Percentiles of the $S_{alluvial}/S_{topset}$ ratio of 2.5, 10, 25, 50, 71 and 75 were used to define model scenarios. Model alluvial slopes were calculated from these ratios using a constant downstream slope ($S_{downstream} = 0.000375$) similar to that of the Atchafalaya Bay, Mississippi delta, Louisiana (Edmonds and Slingerland, 2010). During the simulation, both alluvial ($S_{alluvial}$) and downstream slope ($S_{downstream}$) evolved and created delta plains with varying topset slope values (S_{topset}), as aggradation occurred (Video S1). We defined equilibrium to have been reached when there was constant sediment discharge and channel depth at the model inlet after ~3-6 days of simulation time.
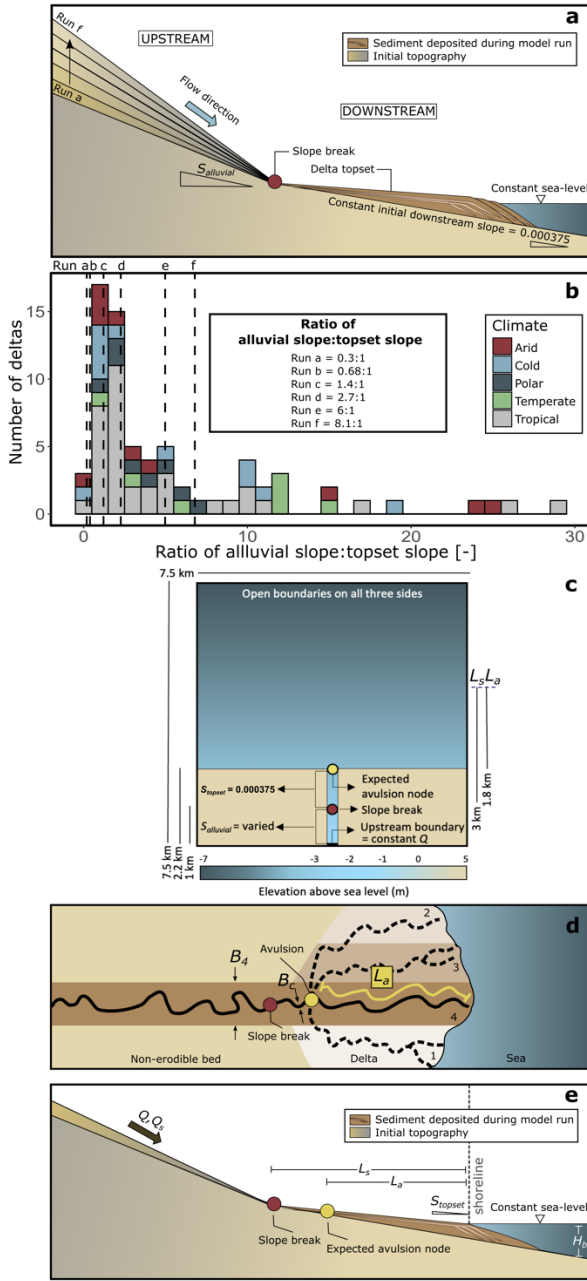
Figure 1: (a) Schematic diagram of the model design. The alluvial slope of each run was calculated from six percentiles from the alluvial slope-topset slope ratios of modern river deltas shown in Fig. 1b. Initial downstream slope is kept constant at 0.000375, adopted from the downstream slope of the modern Mississippi delta (Edmonds and Slingerland, 2010). (b) Distribution of the ratio between alluvial ($S_{alluvial}$) and topset slopes (S_{topset}) from 105 modern river deltas distributed across five climate regions. Ratios used for numerical model runs are indicated by vertical dashed lines. (c) Plan view of the model design. L_s and L_a are slope break and avulsion lengths, respectively. The non-erodible bed at 5 m above sea level represents non-erodible bedrock. (d) Schematic diagram of a river delta showing avulsion location, inlet sediment supply (Q_s), lobe width of each avulsion (B), avulsion length (L_a) and channel widths measured at avulsion (B_c), modified from Chadwick et al. (2020). Numbers near the shoreline represent the number of delta lobes that were used to measure B; e.g. B_4 on (d) represents

 the width of the fourth lobe built. (e) Schematic cross-section showing basin depth (H_b) and topset slope (S_{topset}). Parameters shown in Fig. 1d-e are measured at each timestep during delta growth.

2.2 Model setup

We used Delft3D software to model six scenarios. Delft3D is a physics-based model that simulates hydro-morphodynamics and has been validated for a wide range of environments, including reach-scale meandering and braided rivers, estuaries, and self-formed river deltas (Edmonds and Slingerland, 2007, 2008; Geleynse et al., 2011; Leuven et al., 2023; Morgan et al., 2020; Nienhuis et al., 2018a; Nijhuis et al., 2015; Rossi et al., 2016; Williams et al., 2016). Delft3D solves the shallow water equation and is integrated with the D-Morphology sediment transport and morphology module (Deltares, 2021). Delft3D calculates the flow velocity, sediment transport and update the bed levels at each computational timestep by calculating bed sediment mass for each cell as the results of suspended and bedload transport divergence (Deltares, 2021).

Table 1: Numerical modelling scenarios as defined in Fig. 1.

Run ID	Percentile from $S_{alluvial}$ to S_{topset} ratio	Initial alluvial slope, $S_{alluvial}$	Initial downstream topset slope, S_{topset}	Ratio of alluvial slope to downstream topset slope
a	2.5	1.13×10^{-4}	3.75×10^{-4}	0.30
b	10	2.55×10^{-4}	3.75×10^{-4}	0.68
c	25	5.25×10^{-4}	3.75×10^{-4}	1.4
d	50	1.01×10^{-3}	3.75×10^{-4}	2.7
e	71	2.25×10^{-3}	3.75×10^{-4}	6.0
f	75	3.04×10^{-3}	3.75×10^{-4}	8.1

The alluvial slope was the only controlled variable in our study, with all other setup and parameters were the same as 'scenario o' of Edmonds & Slingerland (2010) and Caldwell & Edmonds (2014) (Fig. 1c). The model domain was rectangular with four boundaries, the incoming river discharge being located at the 'South' boundary of the model and the other three boundaries set to 0 m elevation above sea level (Fig. 1c). The constant incoming river discharge, set at 1050 m^3 s^{-1}, was uniformly distributed across the 250 m wide inlet channel, and inlet sediment discharge was in equilibrium with transport capacity. Various alluvial slopes were achieved by changing the inlet channel elevation in each run while maintaining the receiving basin's depth. Consequently, sediment discharge varied in each run because of the varied alluvial slope as the main controlled variable in the experiments. Our modelled deltas closely represented natural deltas because the discharge ratio and the differences in bed heights between bifurcating distributary channels follow ranges similar to those reported for natural deltas (Edmonds & Slingerland, 2010). Sea-level remained constant within the model, and no subsidence, tide or wave effects were considered.

The model domain was 7.5 km x 7.5 km to avoid the delta plain extending across the model boundaries. Click or tap here to enter text.Constant sediment grain-size distributions were used throughout the model. Fine sand was introduced as non-

125 cohesive sediment (D_{50} = 125 μm with a Gaussian distribution) and medium-grained silt was introduced as cohesive sediment (D_{50} = 30 μm). The critical bed shear stress for erosion = 0.10 N m^{-2} and the model initially contained 5 metres of fully mixed sediments. We introduced a slope break 1 km from the inlet boundary to drive delta formation in the model's initial bathymetry. Using the slope break-avulsion length scaling identified from measured global river deltas (Prasojo et al., 2022) the expected first avulsion node location should emerge in each scenario at around 2.2 km from the inlet (Fig.1c). Other physical and

130 numerical parameters were held constant across all scenarios (Table 2).

For 18 days simulation, the model produced one output every 480 minutes resulting in 52 visualisation outputs (i.e. maps) at the end of the simulations. Using a morphological scale factor (*morfac*) of 175, these 52 maps represented 3150 days (8.6 years) of prototype time. Because bankfull discharge occurs for c.2% of time on average (Dunne & Leopold, 1978), 18 days of simulation thus represent around 430 years of 'real' time (i.e. 8.6 years divided by 0.02).

135 **Table 2:** User-defined model parameters (adopted from Edmonds & Slingerland (2010); Caldwell & Edmonds (2014)).

Parameter	Value	Units
Grid size	300 x 300	cells
	7.5 x 7.5	km
Cell size	25 x 25	m
Run duration	18	days
'Real time' converted run duration	430	years
Basin bed slope (downstream of slope break)	0.000375	(-)
Initial channel dimension (width x depth)	250 x 2.5	m
Upstream non-erodible bed elevation	5	m
Initial channel length upstream of slope break	1000	m
Initial avulsion length from the expected shoreline	1800	m
Water discharge	1050	m^3.s^{-1}
Constant water surface elevation at downstream open boundary	0	m
Initial sediment layer thickness at bed	5	m
Number of subsurface stratigraphy bed layers	1	(-)
Computational time step	0.2	min
Output interval	480	min
Morphological scale factor	175	(-)
Spin-up interval	1440	min

2.3. Surface morphological metrics

The model reached equilibrium after ~3-6 days of simulation time when we begin measurements of morphometric variables and avulsion timescale. Avulsion timescale, defined as the time in between successive avulsions, was empirically measured throughout all experiments after equilibrium was attained. Avulsions were defined when a distributary channel produced during delta formation changed its course and commenced deposition of a new delta lobe. We only considered avulsions caused by progradation or incision that are common in river deltas (Slingerland and Smith, 2004). The timing of each avulsion in the model was noted and converted to a 'real' time as $T_{a\ empirical}$.

Numerous morphological surface metrics can be used to describe delta form. The surface metrics used here followed those used in an analytical solution for avulsion timescale (Eq. (4) from Chadwick et al., 2020), which utilised delta lobe width (B), channel width at avulsion (B_c), avulsion length (L_a), basin depth (H_b), magnitude of relative sea-level rise (z), topset slope (S_{topset}), bankfull depth (h_c) and sediment supply (Q_s). Avulsion length, delta lobe width, channel width at avulsion and delta topset slope were measured on all maps after equilibrium is reached. The delta lobe width, channel width at each avulsion node and avulsion length were measured in QGIS from the georeferenced images produced by Delft3D (Fig. 1d, Table S1). Delta lobe width was measured as the maximum width of each lobe, while avulsion length was measured along the longest channel from the shoreline to the most upstream avulsion node located at the 'expected avulsion node' defined in Fig. 1c. Topset slope (S_{topset}) was calculated as the average slope of a delta plain. To measure S_{topset}, digital elevation models (DEMs) for each timestep were first extracted from Delft3D and then cropped to only cover the delta plain. We then filtered the DEM to only include elevation, z between 0-5 metre ($0 < z < 5$) to cover that part of the delta plain that is exposed above sea-level (i.e. $z = 0$ m) but below the non-erodible bed (i.e. $z = 5$ m; Fig. 1d). After cropping and filtering, the DEM was then transformed to a slope raster defined as the change of elevation for each DEM cell in x and y directions with $S_{topset} = \sqrt{\left(\frac{dz}{dx}\right)^2 + \left(\frac{dz}{dy}\right)^2}$. The mean topset slope for each timestep was then extracted from the slope raster as the slope values for each scenario show unimodal distributions (Table S1; Fig. S1). Lastly, the sediment load (Q_s) at the channel inlet was obtained from the QUICKPLOT (v2.60.65942) Delft3D visualisation software.

Bankfull depth (h_c) was calculated using Eq. (1) (Parker, 2007).

$$h_c = \left(\frac{C_f Q^2}{g B_c{}^2 S_{topset}}\right)^{\frac{1}{3}}, \tag{1}$$

where C_f is a bed friction coefficient [-] = 0.002 for large lowland rivers (Parker et al., 2007), Q = bankfull discharge [$m^3\ s^{-1}$] = 1050 $m^3\ s^{-1}$, and g = gravitational acceleration [$m\ s^{-2}$] = 9.81 $m\ s^{-2}$.

The avulsion timescale was calculated between each successive pair of avulsions observed in the model ($T_{a\ empirical}$) and was correlated with all the measured morphometric variables (e.g. Q_s, L_a, B_c, B, S_{topset}, $S_{alluvial}$, and h_c) from all post-equilibrium maps. Scatter plots and Pearson correlation coefficients (r) were used to assess the shape of relationships and potential dependencies between all variables.

2.4. Comparing numerical model to analytical solution and natural deltas

We used Chadwick et al.'s (2020) mass-balance based analytical solution to calculate expected avulsion timescales for our model conditions (Eqs. (3-6), Table S1). Measured independent surface morphological metrics were used in Eqs. (3-6) to calculate avulsion frequency (f_a) and timescale (T_a).

$$f_a = \frac{1}{T_a} = \frac{1}{(1-\lambda_p)} \frac{Q_s}{(L_a - D)BH + DB\left(H_b + z + \frac{DS_{topset}}{2}\right)} \; if \; D \geq 0, \tag{3}$$

$$f_a = \frac{1}{T_a} = \frac{1}{(1-\lambda_p)} \frac{Q_s}{L_a BH} \; if \; D < 0, \tag{4}$$

$$D = (H - z)/S_{topset}, \tag{5}$$

$$H = H^* h_c, \tag{6}$$

with f_a = avulsion frequency [year^{-1}], Q_s = sediment load [m^3 s^{-1}], λ_p = sediment porosity [-], L_a = avulsion length [m], D = delta lobe-progradation distance [km], B = delta lobe width of each avulsion [m], H = aggradation thickness necessary for avulsion [m], H_b = basin depth [m], z = magnitude of sea level rise during an interavulsion period [m], S_{topset} = topset slope [-], H^* = avulsion threshold [-], and h_c = bankfull depth [m] calculated using Eq. (1).

In calculating these analytical avulsion timescales, sensitivity analyses were undertaken using avulsion thresholds (H^*) of 0.2, 0.5, and 1.4, which are realistic for lowland deltas (Ganti et al., 2019), and $D > 0$ since there is no allogenic forcing that would make the delta regress. The analytical avulsion timescales for H^* = 0.2, 0.5, and 1.4 are $T_{a \; H^* = 0.2}$, $T_{a \; H^* = 0.5}$, and $T_{a \; H^* = 1.4}$, respectively (Table S1). Since sea-level is constant in this study, sea level rise $z = 0$. Sediment porosity (λ_p) is assumed to be 0.4 (Jerolmack, 2009; Paola et al., 2011), bed friction coefficient (C_f) = 0.002 for lowland rivers (Parker et al., 2007), and constant bankfull discharge (Q) = 1050 m^3 s^{-1}. Analytical avulsion timescales were then compared to avulsion timescales observed from 19 natural river deltas, two fan deltas and one downscaled physical laboratory fan delta documented in Chadwick et al. (2020) and Jerolmack & Mohrig (2007), using topset slope values from Prasojo et al. (2022) (Table S2).

3. Results

Figure 2 shows the morphology of the deltas in each scenario at the final timestep. Overall, the different alluvial slopes are associated with delta plains that exhibit different shoreline configurations, different numbers of active distributary channels and slightly different delta plain sizes. One delta plain reached the model boundary (Run f, Fig. S2) and this scenario was repeated with a larger domain size and the avulsion timescales and morphological metrics were observed from this larger domain.
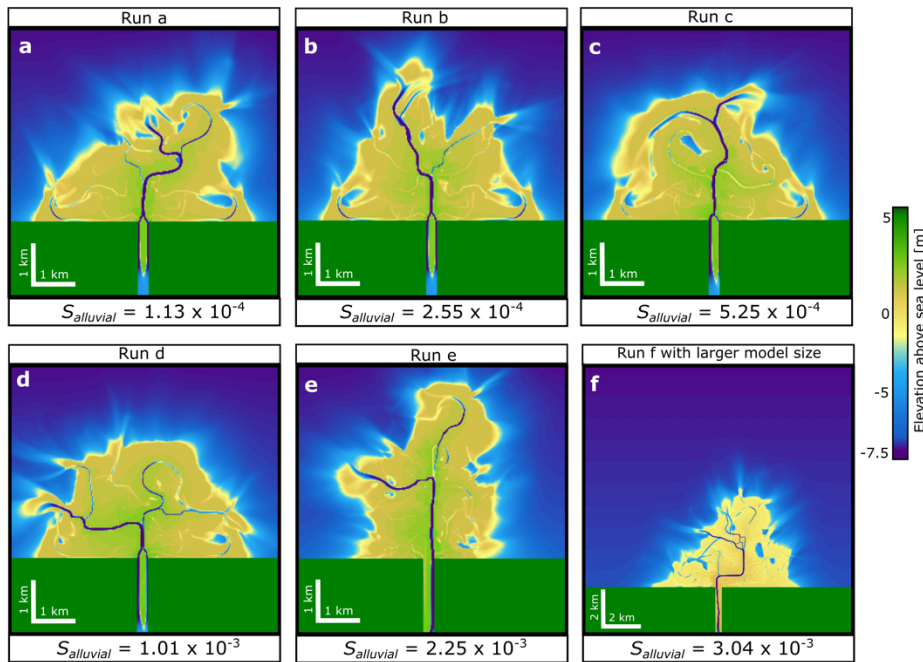
190 **Figure 2:** (a-f) River deltas for each run at the final simulation timestep. Run f uses a larger (12.5 x 12.5 km) model domain to avoid the delta plain reaching the model's boundary. Morphometric measurements for Run f were made on this larger domain.

As an example of avulsion in the model, Figure 3 shows one avulsion that was initiated by an increase of in-channel deposition in a distributary channel around the proto avulsion node (Fig. 3a-b). In-channel aggradation increases the likelihood of overbank flows as it elevates the distributary channel above the surrounding floodplain. Aggradation continued until the levee is breached as the surrounding delta plain provides a lower path for a distributary channel to flow (Fig. 3c). This newly avulsed channel then distributed more water and sediment away from the initial distributary channel path (Fig. 3e-g). A significant increase in post-avulsion sediment thickness around the avulsion node characterises how sediment is now distributed to this newly avulsed channel (Fig. 3h). Note also that bifurcation at the delta shoreline occurred at the same time as the avulsion developed c.1km upstream (Fig. 3b). Bifurcation is initiated by a mouth bar deposition in a more distal part of the delta plain (Fig. 3b). The distributary channel feeding this mouth bar bifurcates once the depth of the mouth bar is ~40% of the initial basin depth, consistent with findings from Edmonds & Slingerland (2007). However, we are uncertain if the mouth bar deposition forces an upstream wave of in-channel deposition that leads to the channel being unstable to trigger an avulsion as the sediment thickness along the avulsing distributary channel remains similar through time (Fig. 3a-g).
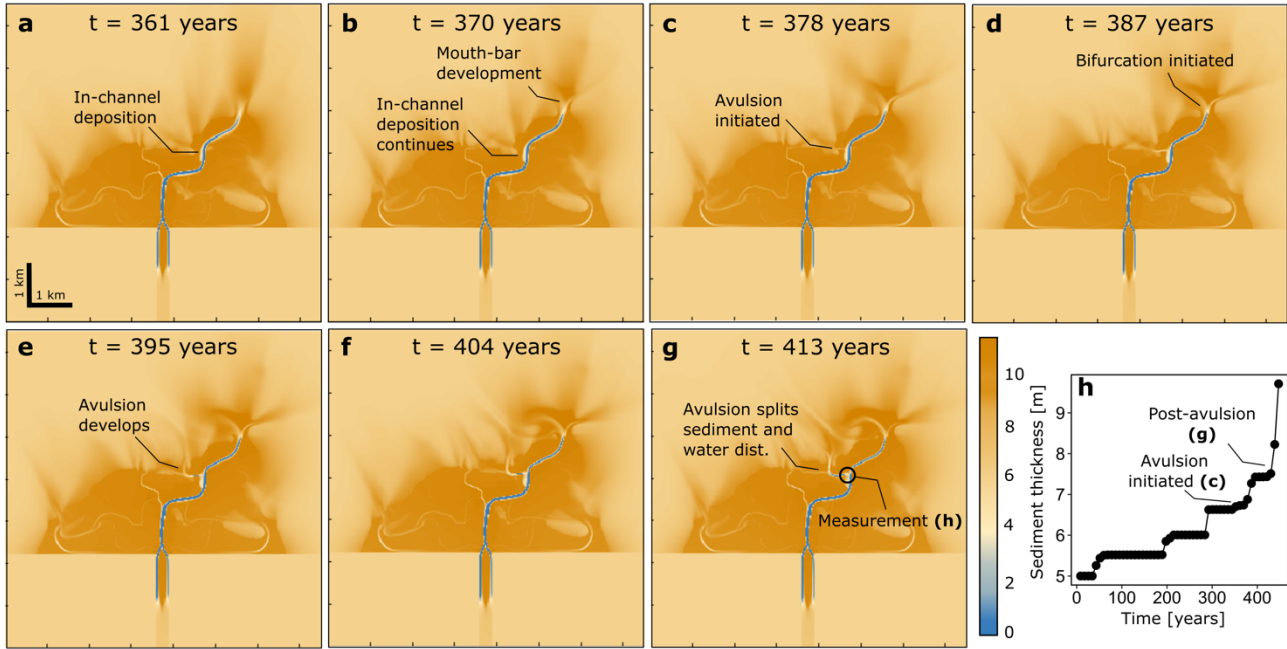
Figure 3: Time series images from Run a showing the detail of an avulsion process (a-g). Time series sediment thickness at the avulsion node (h).

Avulsion occurs as often as every 8.27 years in all scenarios with the maximum time between successive avulsions being 148.9 years (run d). At the upper limit, avulsions occurred 14 times (run a & f) and 6 times as the lower limits (run c). A right skewed distribution of avulsion interval was observed in most scenarios (Fig. S3), with medians from 8.3-16.5 years and means 14.8-33.1 years. The median timing of avulsions remains unchanged over runs a-f (Kruskal-Wallis, p > 0.05) (Fig. S3).

Fig. 4 shows Pearson's correlations between observed avulsion timescales in the model ($T_{a\ empirical}$) and the independent morphometric variables measured in each timestep. $T_{a\ empirical}$ has a weak negative correlation with sediment load, Q_s (r=-0.06). The initial alluvial slope ($S_{alluvial}$; Table 1; Fig. 1), defined independently in our approach, controls the sediment load (Q_s; r=0.86) and is responsible in defining the delta avulsion length, L_a (r=0.58; Fig. 4), suggesting that higher transport capacity on a steeper alluvial slope may produce a longer (i.e. more protruding) delta, consistent with the findings from global river deltas (Prasojo et al., 2022). $T_{a\ empirical}$ is also weakly and negatively correlated with bankfull depth, h_c (r=-0.10), suggesting that bankfull depth may not be a good indicator of avulsion timescale. Sediment load (Q_s) influences the delta topset slope (S_{topset}; r=0.37) so higher riverine sediment loads produce steeper delta plains when the basin configuration is similar. Avulsion timescale ($T_{a\ empirical}$) shows no correlation with the delta size represented as delta avulsion length, L_a (r=-0.01), delta lobe width, B (r=-0.09) and channel width at avulsion node, B_c (r=0.04). Note that there are high degrees of autocorrelation within the morphometric parameters used here, for example between bankfull depth (h_c) with channel width at avulsion, B_c (r=-0.95) and with topset slope, S_{topset} (r=-0.71).
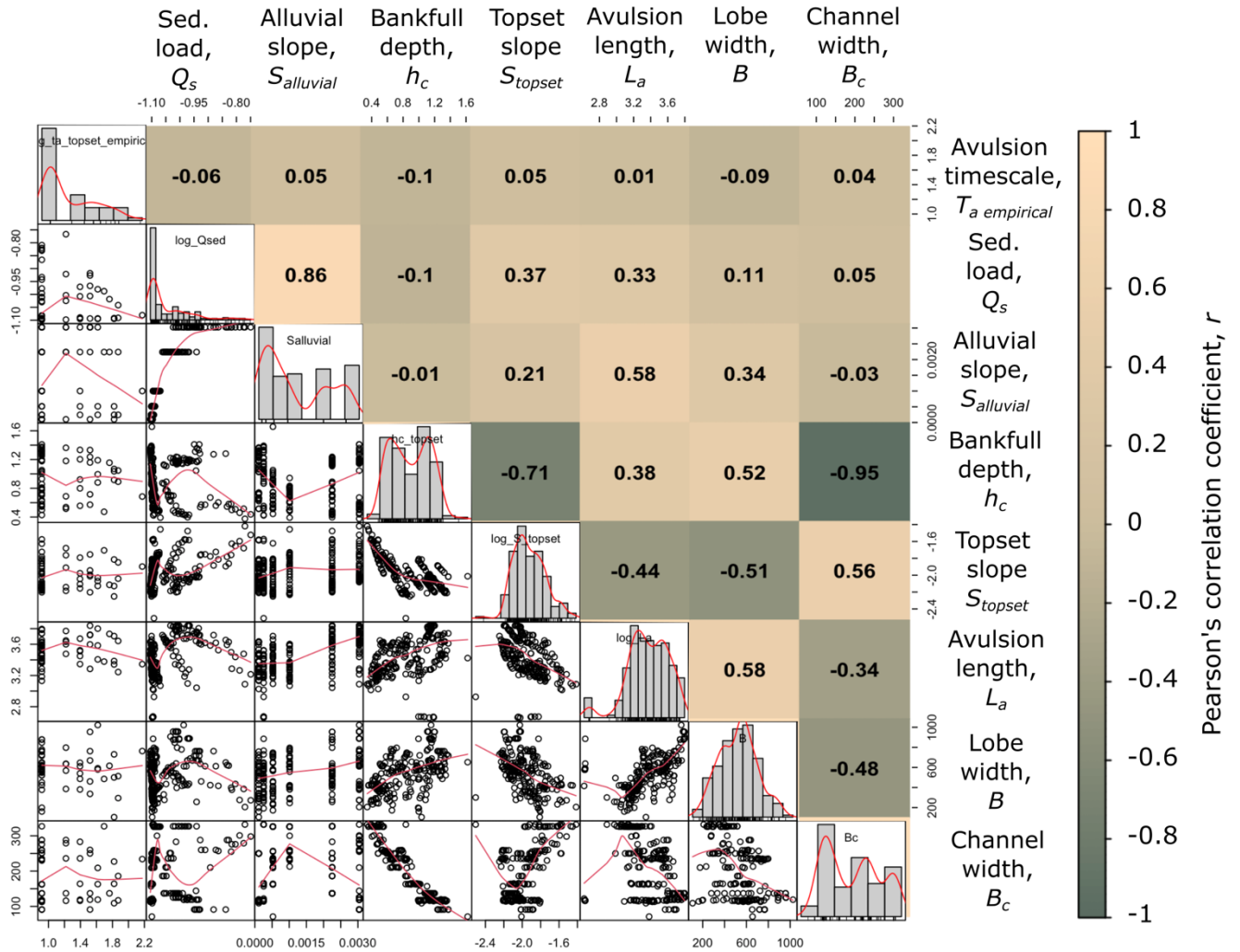
Figure 4: Pearson correlations (upper right panels) between avulsion timescale ($T_{a\ empirical}$) and independent morphometric variables along with their distributions (diagonal panels) and correlations (lower left panels). Units on this figure are years for $T_{a\ empirical}$, m^3 s^{-1} for Q_s, and metres for B_c, h_c and L_a. S_{topset} and $S_{alluvial}$ are dimensionless. Note that h_c is autocorrelated with S_{topset} and B_c as shown in Eq. (1) and $S_{alluvial}$ is initial alluvial slope available from Table 1 as the independent variable used to define the six experimental scenarios. Red lines on the correlation plots are LOWESS curves. Red lines on the histograms aid visualising the distributions. Also note that $T_{a\ empirical}$, Q_s, S_{topset} and L_a are on log-scales.

As Fig. 4 groups the results together, Fig. 5 shows ordinary least square regressions between sediment load (Q_s), avulsion timescale ($T_{a\ empirical}$), initial alluvial slope ($S_{alluvial}$) and bankfull depth (h_c) produced from each scenario. Avulsion timescale is inversely and non-linearly correlated with sediment load (see R^2 values for each scenario and overall dataset at the bottom of Fig. 5), showing the influence of sediment load in defining avulsion timescale observed in our model (Fig. 5a). The higher the riverine sediment load brought into a delta plain, the faster avulsions occur as shown in Fig. 5a. Conversely, the riverine sediment load is positively correlated with initial alluvial slope (Fig. 5b) showing how initial alluvial slope upstream of a delta plain defines how much riverine sediment is being transported to the delta plain. As we maintain the channel width upstream

of a delta plain to be constant (Fig. 1c), a higher transport capacity in a steeper alluvial slope is able to bring more sediment load (Fig. 5b). Lastly, Fig. 5c shows a weak negative correlation between bankfull depth and sediment load. Negative correlation is expected as the higher the riverine sediment load, the more sediment is deposited on a delta plain, making a steeper delta plain (Fig. 4) and shallower bankfull depth (Fig. 5c).
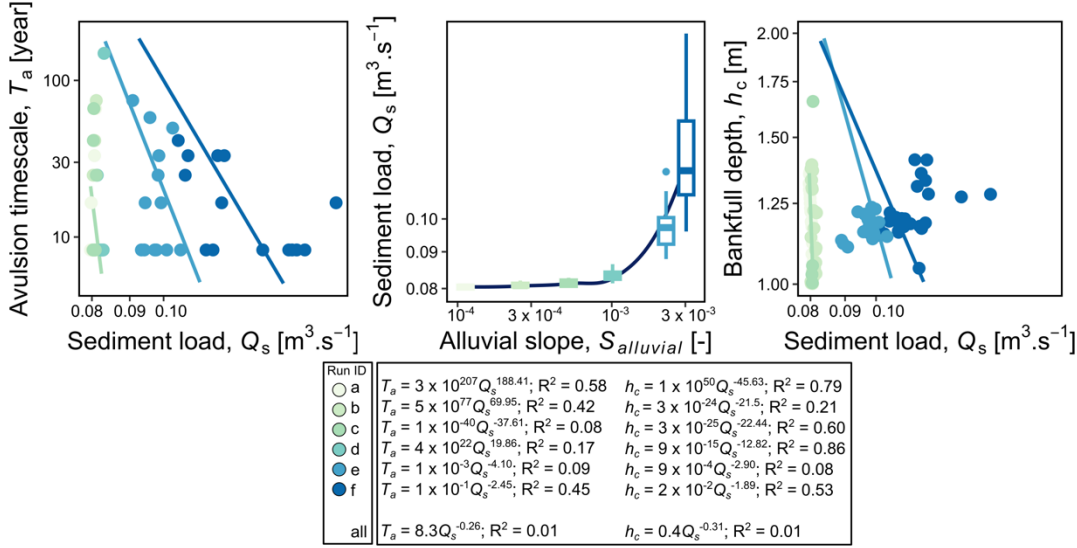
Figure 5: Ordinary least squares log-log regressions and power function equations between avulsion timescale and sediment load (a), sediment load and initial alluvial slope (b) and bankfull depth and sediment load (c) measured from the model (N = 62) plotted on log-log scale.

4. Discussion

Since avulsion is infrequent, and often beyond human monitoring timescales, it is difficult to acquire data sets on avulsion frequency from field studies, except for a few well-documented cases (Moodie et al., 2019; Chamberlain et al., 2018; Pierik et al., 2018; Jerolmack, 2009; Li et al., 2022). The six scenarios modelled in this study have merit in providing a large data set from which to infer the process controls over avulsion timescales.

4.1. Investigating variables controlling avulsion timescales

In this study, to assess the impact of sediment input from the delta's catchment only the initial alluvial slope ($S_{alluvial}$) was varied. All the other measured variables are from these experiments, in which deltas were allowed to self-form. Our experimental set-up determines that initial alluvial upstream slope controls how much sediment enters the delta plain (r=0.8, Fig. 4, Table 3). A steeper initial alluvial slope ($S_{alluvial}$) has a higher transport capacity and so transports a greater sediment load (Q_s), which is then deposited on the delta plain. Higher sediment load results in higher vertical aggradation rate (v_a) in the distributary channel (Chadwick et al., 2020) which elevates the distributary channel floor above its surrounding floodplain. The higher the distributary channel floor relative to the floodplain, the easier it is for an avulsion to occur (Jerolmack and

Mohrig, 2007; Mohrig et al., 2000). While sediment load is controlled by the steepness of the initial alluvial slope transporting the sediment, we propose that the avulsion timescale in our model is influenced by the amount of sediment deposited in a delta plain. Other investigations that have also found that sediment mass-balance is the primary control on avulsion timescales include a radially averaged model (Muto, 2001; Muto & Steel, 1997), a channel-averaged model (Reitz et al., 2010), and backwater-scaled models (Chadwick et al., 2019; Moodie et al., 2019).

Table 3: Average sediment load and initial alluvial slope for each scenario.

Run ID	Initial alluvial slope, $S_{alluvial}$ [-]	Average sediment load, Q_s [m^3.s^{-1}]
a	1.13×10^{-4}	0.0804
b	2.55×10^{-4}	0.0809
c	5.25×10^{-4}	0.0814
d	1.01×10^{-3}	0.0835
e	2.25×10^{-3}	0.0973
f	3.04×10^{-3}	0.1243

4.2. Comparison with analytical solution and natural deltas

Figure 6 shows avulsion timescale scaling relationships observed from our model compared to natural deltas, a physical laboratory fan delta and analytical solutions. Generally, the pattern and magnitude observed from our numerical model are in good agreement with natural and physical laboratory deltas. By bringing natural and physical laboratory deltas that have a larger range of measured variables (e.g. S_{topset}, h_c, B, Q_s, etc), clearer correlations between measured variables and avulsion timescale can now be observed. Topset slope negatively correlates with avulsion timescale, showing a steeper delta plain will experience a faster avulsion (Fig. 6a). Positive correlations between bankfull depth, delta lobe width, avulsion length and avulsion timescale are also consistent between our model and the natural and physical laboratory deltas (Fig. 6b-d). This demonstrates that avulsion takes longer in larger deltas. However, channel width at avulsion, sediment load and avulsion timescale do not show clear patterns (Fig. 6e,f). Additionally, analytical solutions indicate underestimation of avulsion timescale by several orders of magnitudes in comparison to our model, natural and physical laboratory deltas.

A strong negative correlation between avulsion timescale ($T_{a\,empirical}$) and delta topset slope (S_{topset}) shown in Fig. 6a allows a parallel comparison to be made with avulsion controls in comparable alluvial sedimentary environments (e.g. alluvial fans and fan deltas). Diverse alluvial fan and fan delta experiments have shown that avulsion timescale is influenced by fan-channel gradient (equivalent to delta topset slope in our model) (Schumm et al., 1987; Whipple et al., 1998; Van Dijk et al., 2012; Leenman & Eaton, 2021). Fan-channel slope is dependent on sediment flux (Parker et al., 1998; Bagnold, 1986) and sediment flux also influences the avulsion timescale as shown earlier in our model. Consequently, avulsion timescale also has a strong correlation with the fan-channel slope or delta topset slope. However, we propose that delta topset slope is a causal effect of

the amount of sediment fed into a delta plain in our model. As the initial alluvial slope ($S_{alluvial}$) controls the sediment load (Q_s) feeding a delta plain which in turn determines S_{topset}, we argue that $S_{alluvial}$ plays a more fundamental role than S_{topset} in influencing the avulsion timescale ($T_{a\ empirical}$) observed in our model.

285   We consider that results from our analytical-numerical model and natural-physical laboratory deltas are directly comparable, but care is needed in their interpretation. The analytical calculations are for fixed values of input variables, and field data are snapshots assumed to represent equilbria. Conditions change during our numerical model runs, and topset slopes reduce through time (Fig. S4a) which would be expected to lead to an increase in avulsion timescale as the delta grows. This results from gentler topset slopes having reduced transport capacities, which reduces the sediment flux, so reducing the in-channel

290   aggradation rate as explained before (Fig. 6a). Similarly, as bankfull depth is also calculated based on the topset slope value (Eq. (1)), disagreement between analytical and numerical model results is expected (Fig. 6b). Moreover, delta lobe width (B) and avulsion length (L_a) in the original analytical solution are assumed to be constant with $B=40B_c$ and $L_a=0.2L_b-0.5L_b$ (Chadwick et al., 2020). As we found that delta lobe width (B) and avulsion length (L_a) grow through time (Fig. S4b,c) in our numerical model, analytical model assumptions lead to this disagreement (Fig. 6c,d). Compilation of our numerical model

295   with natural and physical laboratory deltas shows that avulsion becomes less frequent in a larger delta (Fig. 6c,d).
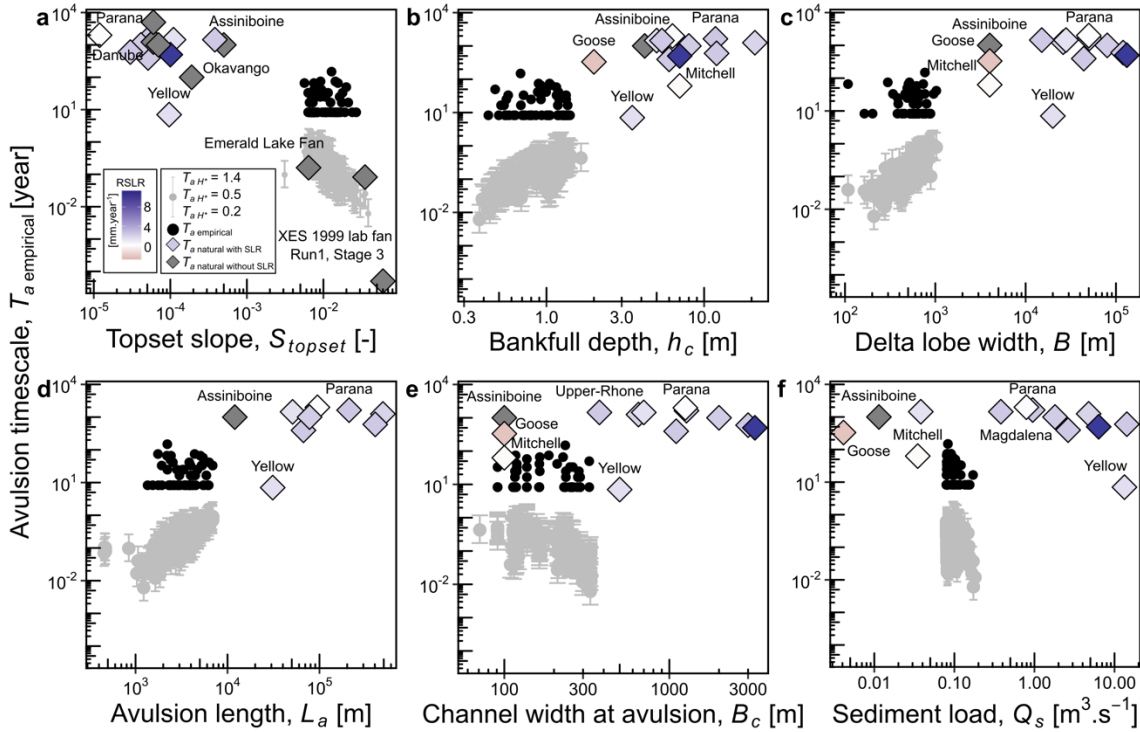
Figure 6: Relationships between avulsion timescales and independent variables: (a) topset slope; (b) bankfull depth; (c) delta lobe width; (d) avulsion length; (e) channel width at avulsion; and (f) sediment load. The plots show model values ($T_{a\ empirical}$) as solid black circles. Grey dots and bars are results from the analytical equations using three avulsion threshold $H*$ values ($T_{a\ H*=1.4}$, $T_{a\ H*=0.5}$, $T_{a\ H*=0.2}$). Diamonds

300   are results from natural and laboratory deltas: grey diamonds indicate examples for which no information about their relative sea-level

changes is available; purple diamonds are for deltas with relative sea-level rise (*RSLR*; mm yr^{-1}) colour-coded as shown. Data from natural deltas and the laboratory experiment are available in Table S2.

The negative correlation between Q_s and T_a from our numerical model (Fig. 5a) deviates from empirical data gathered from natural deltas (Fig. 6f). Natural deltas have relatively larger delta plain sizes than our numerical models represented by avulsion
305   length, bankfull depth and delta lobe width values (Fig. 6b-d). Assuming no sediment bypass, we normalised sediment discharge to delta size by dividing Q_s by $(L_a.B/2)$ to get a vertical aggradation rate, η [m s^{-1}] . Vertical aggradation rate is then normalised by dividing it by shear velocity, $u^* = \sqrt{gh_cS_{topset}}$ [m s^{-1}] as we are looking at a vertical aggradation rate related to transport capacity of flow, taken as a measure of the ability to remove sediment from a delta plain with no subsidence, η^* [-]. Using this dimensionless aggradation rate, Fig. 7a shows a non-linear negative correlation between $T_{a\ empirical}$ and η^* from
310   both natural deltas and our models, suppporting our argument on sediment discharge influence on avulsion timescale. The best-fit equation for this relationship is $T_{a\ empirical} = -231.5\ \ln(\eta^*) - 3573.6$ ($R^2 = 0.71$; $p < 0.05$). At $\eta^* = 2.10^{-7}$ the avulsion timescale becomes 0 (Fig. 7a) implying that at very high aggradation rates, with correspondingly high sediment loads, avulsion will occur effectively instantaneously on a delta plain as the sediment will keep accumulating with very little being removed. Consequently, the flow becomes a random sheet of constant deposition, channel switching and instantaneous avulsion.
315   On the other hand, the range of initial alluvial slopes used in the model, although based on observed slopes from 105 global deltas, does not cover the entire range of Q_s inputs to natural deltas (Fig. 6f). Fig. 7b shows that a significant increase in Q_s (and a resultant decrease in avulsion timescale) would require the initial alluvial slope to be 6 times the initial downstream slope (Table 1, 3). Further simulations, using a different initial downstream slope value or more varied slope ratios, could enable a larger range of Q_s to be covered and hypothetically enable a closer agreement between natural deltas and numerical
320   models (Fig. 6f).
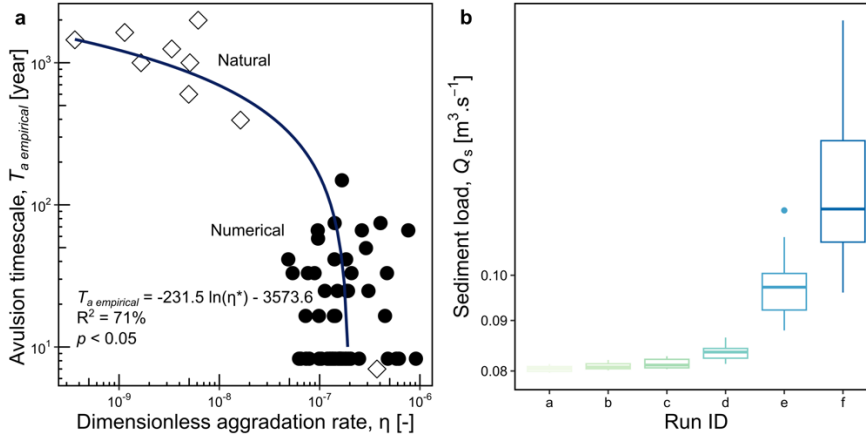
Figure 7: (a) Relationship between avulsion timescale (T_a) and dimensionless aggradation rate (η^*) observed from our natural deltas and our models. Regression lines are shown in blue with 95% confidence band in grey. (b) Boxplots showing distribution of sediment load (Q_s) for each scenario.

325 The bathymetry of the basin is defined at the beginning of our model runs (Fig. 1). The bathymetry adjusts during a model run to reach an equilibrium profile at a simulation timestep > 3-6 days (Video S1). In comparison to other models in which "reference profiles" and their evolution are defined by making assumptions (e.g. floodplain deposition is assumed to be equal to riverbed aggradation) (Chadwick et al., 2019; Moodie et al., 2019; Moran et al., 2017; Ratliff et al., 2018; Edmonds et al., 2022), our approach directly evaluates avulsion frequency and location that emerge from the physics of self-forming delta-

330 lobes. Avulsions in our models consistently arise from channel superelevation (Fig. 1c), consistent with our previous global empirical study (Prasojo et al., 2022).

The ratios between alluvial and topset slope gathered from natural deltas (Table 1) are assumed to be in dynamic equilibrium with the environmental conditions in our study. Even though most modern global deltas have developed since the early Holocene, inevitable natural and anthropogenic changes of boundary conditions such as changes in sediment or water discharge

335 and local sea-level rise will have happened, and remain ongoing, during this period (Stanley & Warne, 1994). The slope data derived from remote sensing only represents a single snapshot of a slope that is constantly evolving towards equilibrium with boundary conditions. Consequently, our measured topset slopes from natural deltas may represent a transient condition rather than being equilibrium values. Repeating the work with different initial topset slope presents an opportunity for further investigation.

340 The avulsion timescales calculated for natural deltas ($T_{a\ natural}$) do not correlate well with relative sea-level rise rate ($RSLR$) (Fig. 6a-f and Fig. S5) (Chadwick et al., 2020). This result supports the hypothesis that the frequency of avulsions may be unaffected by sea-level rise, as also found in an earlier numerical model study (Ratliff et al., 2021) and a global empirical study (Colombera & Mountney, 2023). We propose that avulsion frequency and location are dominated by upstream forcing (i.e. alluvial slope or catchment sediment supply, Fig. 4-7a) (Prasojo et al., 2022) rather than downstream forcing by sea-level rise

345 or backwater effects (Fig. S6) (Chadwick et al., 2020; Chatanantavet et al., 2012; Ganti et al., 2016b). As our deltas are self-formed and evolve throughout the simulations, avulsion and backwater lengths (as a function of topset slope, Eq. (1)) grow linearly and each scenario has a unique avulsion-backwater length ratio (Fig. S6), rather than being constant as previously observed (Ganti et al., 2016; Chatanantavet et al., 2012). Avulsions in the proximal parts of deltas are controlled by upstream forcing, with RSLR and backwater hydraulics determining avulsion frequency only in distal zones, the size of which depends

350 on the magnitude of RSLR and on delta slope.

Previous literature on the relationship between the frequency of avulsion and sea-level rise is somewhat equivocal. A field study conducted on the Mitchell River delta, Australia found that avulsion frequency increases with sea-level fall (Lane et al., 2017). Numerical model results suggest that avulsions on the Mississippi (faster) and Trinity (slower) Rivers showed different responses to Holocene sea-level rise even though they are geographically adjacent (Chatanantavet et al., 2012; Moran et al.,

355 2017). An example during sea-level fall from the Goose River delta, Canada, shows that avulsion frequency remained constant during this base-level adjustment (Nijhuis et al., 2015). In contrast, avulsion frequency in the Rhine-Meuse delta, Netherlands, increased during the Holocene sea-level rise period (Törnqvist, 1994), possibly due to aggradation rate (v_a) being controlled

by *RSLR*. Our experiments do not address this issue, and we propose that further investigations combining numerical and flume experiments that are based on observations from natural deltas may aid resolution of this debate.

4.3. Implications for delta management

Our modelling results advance our understanding of how sediment input from the catchment regulates the timing of avulsions in river deltas. The complex hydraulic and sediment transport processes that lead to the correlation between alluvial slope and avulsion timescale are linked to sediment load, the rate of in-channel aggradation and how rapidly channels become perched. Consequently, with the increase of anthropogenic forcing both directly within river deltas and throughout upstream catchment areas (Best, 2019; Darby et al., 2015; Dunn et al., 2019; Hackney et al., 2020), river delta managers can use sediment load management to reduce the risk of avulsion-driven flooding.

However, finding a perfect balance between reducing avulsion frequency, maintaining the sediment load required to nourish delta environments and to hinder deltas' risk from subsidence and coastal erosion, is challenging. In some locations, deforestation that increases sediment supply is responsible for c.25% of net land gain on global deltas, which may also hasten future avulsions (Nienhuis et al., 2020). Conversely, river impoundment is responsible for more than a 50% reduction in sediment delivery to the global ocean since 1950, collectively leading to a loss of a delta land of 127 ± 8.3 km^2 annually over the 30 years from 1980-2010 (Nienhuis et al., 2020). This declining sediment input not only poses threats to the long-term sustainability of deltas but also renders them susceptible to adverse effects from rising sea levels and ecological degradation due to sediment starvation and saltwater ingress (Jordan et al., 2019). Therefore, gaining insights into the distribution patterns and quantities of sediments in deltas is imperative to ensure their continued sustainability.

4.4. Next steps

An important extension of this modelling work is to have more varied $S_{topset}:S_{alluvial}$ ratios, water discharge (Q) and sediment load (Q_s), as variability in these may affect the geomorphic processes controlling avulsion timescale. Moreover, investigation using scenarios based on sets of geological variables that control slopes, rather than varying the slopes themselves will be regarded as valuable. Multi-temporal observation of well-studied natural river deltas, such as the Yellow (Moodie et al., 2019), Mississippi (Chamberlain et al., 2018) or Rhine-Meuse (Pierik et al., 2018) deltas, could then be used to validate model results. On the other hand, incorporating other variables such as grain size and sediment cohesion, forcing through sea-level rise and subsidence, varying basin geometry and adding vegetation that controls crevassing and consequently increases avulsion timescale in future numerical modelling should be considered and are already in other studies (Nienhuis et al., 2018; Pierik et al., 2023; Sanks et al., 2022). In particular, considering the importance of projected global sea-level changes and the variability of results reported in the literature, a better understanding of sea-level rise impacts on delta avulsion is needed.

We have used a simplified modelling approach and have isolated one predictor variable while holding other factors constant. Observations of the processes and evolution in the numerical deltas shows the complexity of hydraulic and morphodynamic processes across delta plains. Future work will need to address this complexity, including: (a) How does the forcing studied

390 here (alluvial slope and consequent sediment input) interact with a combination of other factors (e.g. sea-level, wave and tidal regimes, and anthropogenic effects)? (b) How do the other controls (e.g. Q_s, Q, riverbank material, vegetation) in river deltas influence avulsion timescales? and, (c) how might these avulsion signals be preserved or shredded in the rock record?

5. Conclusion

We conducted a suite of numerical morphodynamic modelling experiments with variable river alluvial slopes (from 1.13×10^{-4}

395 to 3.04×10^{-3}) to understand the controls over avulsion location and timescale in a river delta. Sediment load, which in this study was controlled by the imposed alluvial slope upstream of a delta plain, controls the avulsion timescale. Mechanistically, when channel width is constant, steeper alluvial slope has a greater sediment transport capacity. Consequently, a steeper alluvial slope may transport a larger sediment load to be delivered to a delta plain. This induces accelerated vertical aggradation that causes more frequent avulsion in our model. Integrating our numerical modelling results with analytical, natural and

400 physical laboratory deltas supports the hypothesis of upstream forcing influencing delta avulsion timescale and location, rather than downstream influence by backwater length or sea-level rise. However, our model has several limitations such as dynamic equilibrium assumption from our alluvial-topset slope ratios, homogeneous initial topset slope adopted from Mississippi delta and constant discharge applied in the model, along with factors that were ignored (e.g. tectonics). An improved understanding of the influence of alluvial slope on the timing of avulsion in river deltas has significant implications due to their direct impacts

405 on: (i) coastal and inland hazards on highly populated river deltas; and, (ii) rock record interpretations.

Data availability

The morphometric variables and avulsion timescales observed from our models are available in Table S1. The dataset from natural and laboratory river deltas used in this study (Table S2) and model scenarios (Run a-f) along with their simulation videos of bed level change and non-cohesive and cohesive sediment concentration distributions from Run a are available in

410 the FigShare repository (Prasojo et al., 2023a,b, 2024).

Author contributions

OAP, TBH, AO and RDW conceptualised the study. OAP and TBH designed the Delft3D simulation. OAP collected the morphometrics from numerical model and natural deltas. OAP wrote the paper, and TBH, AO and RDW reviewed it. All authors discussed the results and contributed to the final article.

415 **Competing interests**

The authors declare that they have no conflict of interest.

Acknowledgements

We thank A.J.F. (Ton) Hoitink, Luca Colombera, Andrew Moodie and other referees of an earlier version who have contributed significantly to improve the quality of this manuscript. For the purpose of open access, the authors have applied a Creative
420 Commons Attribution (CC-BY) licence to any Author Accepted Manuscript version arising from this submission.

Financial support

This study was funded by an Indonesia Endowment Fund for Education (LPDP) awarded to Prasojo.

References

Aslan, A., Autin, W. J., and Blum, M. D.: Causes of river avulsion: Insights from the late Holocene avulsion history of the
425 Mississippi River, U.S.A, Journal of Sedimentary Research, 75, 650–664, https://doi.org/10.2110/jsr.2005.053, 2005.

Bagnold, R. A.: An Approach to the Sediment Transport Problem From General Physics, USGS Professional Paper 422-I, doi:10.3133/pp422i, 1966.

Bates, C. C.: Rational Theory of Delta Formation. AAPG Bulletin, 37(9), 2119–2162, https://doi.org/10.1306/5ceadd76-16bb-11d7-8645000102c1865d, 1953.

430 Best, J.: Anthropogenic stresses on the world's big rivers, Nature Geoscience, 12(1), 7–21, https://doi.org/10.1038/s41561-018-0262-x, 2019.

Brooke, S., Chadwick, A. J., Silvestre, J., Lamb, M. P., Edmonds, D. A., & Ganti, V. Where rivers jump course. Science, 376(6596), https://doi.org10.1126/science.abm1215, 2022.

Brooke, S., Ganti, V., Chadwick, A. J., and Lamb, M. P.: Flood Variability Determines the Location of Lobe-Scale Avulsions
435 on Deltas: Madagascar, Geophys Res Lett, 47, e2020GL088797, https://doi.org/10.1029/2020GL088797, 2020.

Caldwell, R. L. and Edmonds, D. A.: The effects of sediment properties on deltaic processes and morphologies: A numerical modeling study, J Geophys Res Earth Surf, 119, 961–982, https://doi.org/10.1002/2013JF002965, 2014.

Chadwick, A. J., Lamb, M. P., Moodie, A. J., Parker, G., & Nittrouer, J. A.: Origin of a Preferential Avulsion Node on Lowland River Deltas, Geophysical Research Letters, 46(8), 4267–4277, https://doi.org/10.1029/2019GL082491, 2019

440 Chadwick, A. J., Lamb, M. P., and Ganti, V.: Accelerated river avulsion frequency on lowland deltas due to sea-level rise, Proc Natl Acad Sci U S A, 117, 17584–17590, https://doi.org/10.1073/pnas.1912351117, 2020.

Chadwick, A. J., Steele, S., Silvestre, J., & Lamb, M. P.: Effect of Sea-level Change on River Avulsions and Stratigraphy for an Experimental Lowland Delta, Journal of Geophysical Research: Earth Surface, e2021JF006422, https://doi.org/10.1029/2021JF006422, 2022.

445 Chatanantavet, P., Lamb, M. P., and Nittrouer, J. A.: Backwater controls of avulsion location on deltas, Geophys Res Lett, 39, 2–7, https://doi.org/10.1029/2011GL050197, 2012.

Colombera, L., & Mountney, N. P.: Downstream controls on coastal-plain river avulsions: A global study, Journal of Geophysical Research: Earth Surface, 128, e2022JF006772, https://doi.org/10.1029/2022JF006772, 2023.

Darby, S. E., Dunn, F. E., Nicholls, R. J., Rahman, M., & Riddy, L.: A first look at the influence of anthropogenic climate

450   change on the future delivery of fluvial sediment to the Ganges–Brahmaputra–Meghna delta, Environmental Science: Processes & Impacts, 17(9), 1587–1600, https://doi.org/10.1039/C5EM00252D, 2015.

Dunn, F. E., Darby, S. E., Nicholls, R. J., Cohen, S., Zarfl, C., & Fekete, B. M.: Projections of declining fluvial sediment delivery to major deltas worldwide in response to climate change and anthropogenic stress, Environmental Research Letters, 14(8), 084034, https://doi.org/10.1088/1748-9326/AB304E, 2019.

455   Dunne, T. and L.B. Leopold.: Water in Environmental Planning, W.H. Freeman and Company, San Francisco, California, 1978.

Deltares: Delft3D - User Manual, 3.15., Deltares, 1–695 pp., 2021.

Edmonds, D. A., Chadwick, A. J., Lamb, M. P., Lorenzo-Trueba, J., Murray, A. B., Nardin, W., Salter, G., & Shaw, J. B.: Morphodynamic Modeling of River-Dominated Deltas: A Review and Future Perspectives, Treatise on Geomorphology, 110–

460   140. https://doi.org/10.1016/B978-0-12-818234-5.00076-6, 2022.

Edmonds, D. A. and Slingerland, R. L.: Mechanics of river mouth bar formation: Implications for the morphodynamics of delta distributary networks, J Geophys Res Earth Surf, 112, https://doi.org/10.1029/2006JF000574, 2007.

Edmonds, D. A. and Slingerland, R. L.: Stability of delta distributary networks and their bifurcations, Water Resour Res, 44, 9426, https://doi.org/10.1029/2008WR006992, 2008.

465   Edmonds, D. A. and Slingerland, R. L.: Significant effect of sediment cohesion on delta morphology, Nat Geosci, 3, 105–109, https://doi.org/10.1038/ngeo730, 2010.

Edmonds, D. A., Hoyal, D. C. J. D., Sheets, B. A., and Slingerland, R. L.: Predicting delta avulsions: Implications for coastal wetland restoration, Geology, 37, 759–762, https://doi.org/10.1130/G25743A.1, 2009.

Edmonds, D. A., Paola, C., Hoyal, D. C. J. D., & Sheets, B. A.: Quantitative metrics that describe river deltas and their channel

470   networks, Journal of Geophysical Research: Earth Surface, 116(4), 1–15, https://doi.org/10.1029/2010JF001955, 2011.

Ericson, J. P., Vörösmarty, C. J., Dingman, S. L., Ward, L. G., and Meybeck, M.: Effective sea-level rise and deltas: Causes of change and human dimension implications, Glob Planet Change, 50, 63–82, https://doi.org/10.1016/j.gloplacha.2005.07.004, 2006.

Fagherazzi, S., Edmonds, D. A., Nardin, W., Leonardi, N., Canestrelli, A., Falcini, F., Jerolmack, D. J., Mariotti, G., Rowland,

475   J. C., and Slingerland, R. L.: Dynamics of river mouth deposits, Reviews of Geophysics, 53, 642–672, https://doi.org/10.1002/2014RG000451, 2015.

Ganti, V., Chadwick, A. J., Hassenruck-Gudipati, H. J., & Lamb, M. P.: Avulsion cycles and their stratigraphic signature on an experimental backwater-controlled delta, Journal of Geophysical Research: Earth Surface, 121(9), 1651–1675, https://doi.org/10.1002/2016JF003915, 2016.

480   Ganti, V., Chadwick, A. J., Hassenruck-Gudipati, H. J., Fuller, B. M., and Lamb, M. P.: Experimental river delta size set by multiple floods and backwater hydrodynamics, Sci Adv, 2, e1501768, https://doi.org/10.1126/sciadv.1501768, 2016.

Ganti, V., Lamb, M. P., & Chadwick, A. J.: Autogenic Erosional Surfaces in Fluvio-deltaic Stratigraphy from Floods, Avulsions, and Backwater Hydrodynamics, Journal of Sedimentary Research, 89(8), 815–832, https://doi.org/10.2110/jsr.2019.40, 2019.

485   Geleynse, N., Storms, J. E. A., Walstra, D. J. R., Jagers, H. R. A., Wang, Z. B., and Stive, M. J. F.: Controls on river delta formation; insights from numerical modelling, Earth Planet Sci Lett, 302, 217–226, https://doi.org/10.1016/j.epsl.2010.12.013, 2011.

Giosan, L., Syvitski, J., Constantinescu, S., and Day, J.: Climate change: Protect the world's deltas, Nature, 516, 31–33, https://doi.org/10.1038/516031a, 2014.

490   Hackney, C. R., Darby, S. E., Parsons, D. R., Leyland, J., Best, J. L., Aalto, R., Nicholas, A. P., and Houseago, R. C.: River bank instability from unsustainable sand mining in the lower Mekong River, Nature Sustainability 2020 3:3, 3, 217–225, https://doi.org/10.1038/s41893-019-0455-3, 2020.

Hartley, A. J., Weissmann, G. S., and Scuderi, L.: Controls on the apex location of large deltas, J Geol Soc London, 174, 10–13, https://doi.org/10.1144/jgs2015-154, 2017.

495   Jerolmack, D. J.: Conceptual framework for assessing the response of delta channel networks to Holocene sea level rise, Quaternary Science Reviews, 28, 1786–1800, https://doi.org/10.1016/j.quascirev.2009.02.015, 2009.

Jerolmack, D. J. and Mohrig, D.: Conditions for branching in depositional rives, Geology, 35, 463–466, https://doi.org/10.1130/G23308A.1, 2007.

Jones, L. S. and Schumm, S. A.: Causes of Avulsion: An Overview, Fluvial Sedimentology VI, 169–178, 500   https://doi.org/10.1002/9781444304213.CH13, 2009.

Kleinhans, M. G. and Hardy, R. J.: River bifurcations and avulsion, https://doi.org/10.1002/esp.3354, 15 March 2013.

Kleinhans, M. G., Ferguson, R. I., Lane, S. N., and Hardy, R. J.: Splitting rivers at their seams: bifurcations and avulsion, Earth Surf Process Landf, 38, 47–61, https://doi.org/10.1002/esp.3268, 2013.

Lane, T. I., Nanson, R. A., Vakarelov, B. K., Ainsworth, R. B., and Dashtgard, S. E.: Evolution and architectural styles of a 505   forced-regressive Holocene delta and megafan, Mitchell River, Gulf of Carpentaria, Australia, Geol Soc Spec Publ, 444, 305–334, https://doi.org/10.1144/SP444.9, 2017.

Leenman A, Eaton B.: Mechanisms for avulsion on alluvial fans: Insights from high-frequency topographic data, Earth Surface Processes and Landforms, 46, 1111–1127, https://doi.org/10.1002/esp.5059, 2021.

Li, J., Ganti, V., Li, C., & Wei, H.: Upstream migration of avulsion sites on lowland deltas with river-mouth retreat, Earth and 510   Planetary Science Letters, 577, 117270, https://doi.org/10.1016/J.EPSL.2021.117270, 2022.

Loucks, D. P.: Developed river deltas: are they sustainable?, Environmental Research Letters, 14, 113004, https://doi.org/10.1088/1748-9326/AB4165, 2019.

Leuven, J. R. F. W., Niesten, I., Huismans, Y., Cox, J. R., Hulsen, L., van der Kaaij, T., and Hoitink, A. J. F.: Peak Water Levels Rise Less Than Mean Sea Level in Tidal Channels Subject to Depth Convergence by Deepening, J Geophys Res Oceans, 128, e2022JC019578, https://doi.org/10.1029/2022JC019578, 2023.

Loucks, D. P.: Developed river deltas: are they sustainable?, Environmental Research Letters, 14, 113004, https://doi.org/10.1088/1748-9326/AB4165, 2019.

Mohrig, D., Heller, P. L., Paola, C., and Lyons, W. J.: Interpreting avulsion process from ancient alluvial sequences: Guadalope-Matarranya system (Northern Spain) and Wasatch formation (Western Colorado), Bulletin of the Geological Society of America, 112, 1787–1803, https://doi.org/10.1130/0016-7606(2000)112<1787:IAPFAA>2.0.CO;2, 2000.

Moodie, A. J., Nittrouer, J. A., Ma, H., Carlson, B. N., Chadwick, A. J., Lamb, M. P., & Parker, G.: Modeling Deltaic Lobe-Building Cycles and Channel Avulsions for the Yellow River Delta, China, Journal of Geophysical Research: Earth Surface, 124(11), 2438–2462. https://doi.org/10.1029/2019JF005220, 2019.

Moran, K. E., Nittrouer, J. A., Perillo, M. M., Lorenzo-Trueba, J., and Anderson, J. B.: Morphodynamic modeling of fluvial channel fill and avulsion time scales during early Holocene transgression, as substantiated by the incised valley stratigraphy of the Trinity River, Texas, J Geophys Res Earth Surf, 122, 215–234, https://doi.org/10.1002/2015JF003778, 2017.

Morgan, J. A., Kumar, N., Horner-Devine, A. R., Ahrendt, S., Istanbullouglu, E., and Bandaragoda, C.: The use of a morphological acceleration factor in the simulation of large-scale fluvial morphodynamics, Geomorphology, 356, 107088, https://doi.org/10.1016/J.GEOMORPH.2020.107088, 2020.

Muto, T.: Shoreline Autoretreat Substantiated in Flume Experiments, Journal of Sedimentary Research, 71, 246–254, https://doi.org/10.1306/091400710246, 2001.

Muto, T. and Steel, R. J.: Principles of regression and transgression; the nature of the interplay between accommodation and sediment supply, Journal of Sedimentary Research, 67, 994–1000, https://doi.org/10.1306/D42686A8-2B26-11D7-8648000102C1865D, 1997.

Nienhuis, J. H., Ashton, A. D., Edmonds, D. A., Hoitink, A. J. F., Kettner, A. J., Rowland, J. C., & Törnqvist, T. E.: Global-scale human impact on delta morphology has led to net land area gain, Nature, 577(7791), 514–518, https://doi.org/10.1038/s41586-019-1905-9, 2020.

Nienhuis, J. H., Törnqvist, T. E., and Esposito, C. R.: Crevasse Splays Versus Avulsions: A Recipe for Land Building With Levee Breaches, Geophys Res Lett, 45, 4058–4067, https://doi.org/10.1029/2018GL077933, 2018a.

Nienhuis, J. H., Hoitink, A. J. F., and Törnqvist, T. E.: Future Change to Tide-Influenced Deltas, Geophys Res Lett, 45, 3499–3507, https://doi.org/doi.org/10.1029/2018GL077638, 2018b.

Nijhuis, A. G., Edmonds, D. A., Caldwell, R. L., Cederberg, J. A., Slingerland, R. L., Best, J. L., Parsons, D. R., and Robinson, R. A. J.: Fluvio-deltaic avulsions during relative sea-level fall, Geology, 43, 719–722, https://doi.org/10.1130/G36788.1, 2015.

Paola, C., Twilley, R. R., Edmonds, D. A., Kim, W., Mohrig, D., Parker, G., et al.: Natural Processes in Delta Restoration: Application to the Mississippi Delta. Annual Review of Marine Science, 3(1), 67–91, https://doi.org/10.1146/annurev-marine-120709-142856, 2011.

Parker, G., Wilcock, P. R., Paola, C., Dietrich, W. E., & Pitlick, J.: Physical basis for quasi-universal relations describing bankfull hydraulic geometry of single-thread gravel bed rivers. Journal of Geophysical Research: Earth Surface, 112(4). https://doi.org/10.1029/2006JF000549, 2007.

550 Pierik, H. J., Moree, J. I. M., van der Werf, K. M., Roelofs, L., Albernaz, M. B., Wilbers, A., van der Valk, B., van Dinter, M., Hoek, W. Z., de Haas, T., and Kleinhans, M. G.: Vegetation and peat accumulation steer Holocene tidal–fluvial basin filling and overbank sedimentation along the Old Rhine River, The Netherlands, Sedimentology, 70, 179–213, https://doi.org/10.1111/SED.13038, 2023.

Prasojo, O. A., Hoey, T. B., Owen, A., and Williams, R. D.: Slope break and avulsion locations scale consistently in global
555 deltas, Geophys Res Lett, e2021GL093656, https://doi.org/10.1029/2021GL093656, 2022.

Prasojo, O. A., Hoey, T. B., Owen, A., & Williams, R. D.: Supporting Information Table S2: First order controls of avulsion in river deltas [Dataset], Figshare, https://doi.org/10.6084/m9.figshare.20654037.v3, 2023a.

Prasojo, O. A., Hoey, T. B., Owen, A., & Williams, R. D.: Model runs: Influence of alluvial slope on avulsion in river deltas [Dataset], Figshare, https://doi.org/10.6084/m9.figshare.23912625.v2, 2023b.

560 Prasojo, O. A., Hoey, T. B., Owen, A., & Williams, R. D.: Alluvial slope influence on avulsion in river deltas - Run a simulation videos [Video], Figshare, https://doi.org/10.6084/m9.figshare.25470505.v1, 2024.

Ratliff, K. M., Hutton, E. W. H., & Murray, A. B.: Modeling long-term delta dynamics reveals persistent geometric river avulsion locations. Earth and Planetary Science Letters, 559, 116786, https://doi.org/10.1016/j.epsl.2021.116786, 2021.

Reitz, M. D., Jerolmack, D. J., & Swenson, J. B.: Flooding and flow path selection on alluvial fans and deltas, Geophysical
565 Research Letters, 37(6), https://doi.org/10.1029/2009GL041985, 2010.

Rossi, V. M., Kim, W., López, J. L., Edmonds, D., Geleynse, N., Olariu, C., Steel, R. J., Hiatt, M., and Passalacqua, P.: Impact of tidal currents on delta-channel deepening, stratigraphic architecture, and sediment bypass beyond the shoreline, Geology, 44, 927–930, https://doi.org/10.1130/G38334.1, 2016.

Sanks, K. M., Zapp, S. M., Silvestre, J. R., Shaw, J. B., Dutt, R., and Straub, K. M.: Marsh Sedimentation Controls Delta Top
570 Morphology, Slope, and Mass Balance, Geophys Res Lett, 49, e2022GL098513, https://doi.org/10.1029/2022GL098513, 2022.

Schumm, S., Mosley, M.P. & Weaver, W.: Experimental fluvial geomorphology, New York: John Wiley and Sons Inc., 1987

Shields, M. R., Bianchi, T. S., Mohrig, D., Hutchings, J. A., Kenney, W. F., Kolker, A. S., and Curtis, J. H.: Carbon storage in the Mississippi River delta enhanced by environmental engineering, Nature Geoscience 2017 10:11, 10, 846–851,
575 https://doi.org/10.1038/ngeo3044, 2017.

Slingerland, R. and Smith, N. D.: River Avulsions and Their Deposits, Annu Rev Earth Planet Sci, 32, 257–285, https://doi.org/10.1146/annurev.earth.32.101802.120201, 2004.

Stouthamer, E., & Berendsen, H. J. A.: Avulsion Frequency, Avulsion Duration, and Interavulsion Period of Holocene Channel Belts in the Rhine-Meuse Delta, The Netherlands, Journal of Sedimentary Research, 71(4), 589–598,
580 https://doi.org/10.1306/112100710589, 2001.

Syvitski, J. P. M. and Saito, Y.: Morphodynamics of deltas under the influence of humans, Glob Planet Change, 57, 261–282, https://doi.org/10.1016/j.gloplacha.2006.12.001, 2007.

Syvitski, J. P. M., Kettner, A. J., Overeem, I., Hutton, E. W. H., Hannon, M. T., Brakenridge, G. R., Day, J., Vörösmarty, C., Saito, Y., Giosan, L., and Nicholls, R. J.: Sinking deltas due to human activities, Nat Geosci, 2, 681–686, https://doi.org/10.1038/ngeo629, 2009.

Tessler, Z. D., Vorosmarty, C. J., Grossberg, M., Gladkova, I., Aizenman, H., Syvitski, J. P. M., and Foufoula-Georgiou, E.: Profiling risk and sustainability in coastal deltas of the world, Science (1979), 349, 638–643, https://doi.org/10.1126/science.aab3574, 2015.

Törnqvist, T. E.: Middle and late Holocene avulsion history of the River Rhine (Rhine-Meuse delta, Netherlands), Geology, 22, 711–714, 1994.

Valenza, J. M., Edmonds, D. A., Hwang, T., and Roy, S.: Downstream changes in river avulsion style are related to channel morphology, Nat Commun, 11, https://doi.org/10.1038/s41467-020-15859-9, 2020.

Van Dijk, M., Kleinhans, M., Postma, G. & Kraal, E.: Contrasting morphodynamics in alluvial fans and fan deltas: effect of the downstream boundary, Sedimentology, 59(7), 2125–2145, https://doi.org/10.1111/j.1365-3091.2012.01337.x, 2012.

Wallace, D. J., Storms, J. E. A., Wallinga, J., Dam, R. L. V. A. N., Blaauw, M., Derksen, M. S., Klerks, C. J. W., Meijneken, C., Snijders, E. L. S. M. A., Fung, G., Mathematics, A., Talbot, N. L. C., Mcsherry, F., Nissim, K., Smith, A., Syvitski, J. P. M., Kettner, A. J., Overeem, I., Hutton, E. W. H., Hannon, M. T., Brakenridge, G. R., Day, J. W., Vörösmarty, C., Saito, Y., Giosan, L., Nicholls, R. J., Stanley, D., Imminent, A. N., To, T., Popul, C., Syvitski, J. P. M., Fabris, M., Achilli, V., Menin, A., Erban, L. E., Gorelick, S. M., Zebker, H. A., Sea, E., Rise, L., Cavalié, O., Sladen, A., Kelner, M., Nice, U. De, Antipolis, S., De, O., Einstein, A., Reed, D. J., and Day, J. W.: Shrinking and Sinking Deltas : Major role of Dams in delta subsidence and Effective Sea Level Rise, Nat Geosci, 123, 1973–1984, https://doi.org/10.1038/ngeo129, 2014.

Whipple, K. X., Parker, G., Paola, C., & Mohrig, D.: Channel dynamics, sediment transport, and the slope of alluvial fans: Experimental study, Journal of Geology, 106(6), 677–693, https://doi.org/10.1086/516053, 1998.

Williams, R. D., Measures, R., Hicks, D. M., and Brasington, J.: Assessment of a numerical model to reproduce event-scale erosion and deposition distributions in a braided river, Water Resour Res, 52, 6621–6642, https://doi.org/10.1002/2015WR018491, 2016.

Wolinsky, M. A., Edmonds, D. A., Martin, J., & Paola, C.: Delta allometry: Growth laws for river deltas, Geophysical Research Letters, 37(21), https://doi.org/10.1029/2010GL044592, 2010.

Wright, L. D.: Sediment transport and deposition at river mouths: A synthesis, Bulletin of the Geological Society of America, 88(6), 857–868, https://doi.org/10.1130/0016-7606(1977)88<857:STADAR>2.0.CO;2, 1977.